Journal of Applied Electrochemistry (2021) 51:739–752
https://doi.org/10.1007/s10800-021-01537-1

RESEARCH ARTICLE

Effect of nanoscale graphene oxide on the sustained photoelectrochemical cathodic protection performance of the WO_3 nanothorn clusters

Mengmeng Sun[1,2,3] · Zhuoyuan Chen[1,2,3] · Jiangping Jing[1,2,3] · Chang Feng[1,2,3]

Received: 24 August 2020 / Accepted: 18 January 2021 / Published online: 11 February 2021

Abstract

The novel photoelectrochemical cathodic protection technology is actively researched and developed for alleviating severe corrosion of marine metallic materials. And the corresponding sustained photoelectrochemical cathodic protection in the dark, under the collaboration of the electron storage materials, is also developed and optimized. WO_3, as a kind of electron storage material, shows great potential in this area. The WO_3/graphene oxide (WO_3/GO) nanothorn cluster composites were synthesized via solovthermal method. The nanoscale graphene oxide (GO) sheets, added as templates, result in the formation of WO_3 nanothorn clusters in the WO_3/GO composite. The hybrid structure of the WO_3/GO composite was formed when the GO adding amount is 0.2 wt%, denoted as WO_3/GO 0.2. The lattice of WO_3 contracted slightly and the crystallinity of WO_3 was enhanced. The WO_3/GO 0.2 nanothorn cluster composites promote the transfer and storage efficiency of the electrons compared with pure WO_3. The high conductivity of the partly reduced GO leads to a faster electron transfer in the WO_3/GO composite. The sustained photoelectrochemical cathodic protection performance of the WO_3/GO composite under the assistance of TiO_2 (i.e., the coupling of WO_3/GO 0.2-TiO_2) for 304 stainless steel (SS) was promoted. A larger number of photoinduced electrons, generated by TiO_2 under white light illumination, can be stored in the WO_3/GO composite and be transferred to the coupled 304 SS electrode after shutting off the light.

✉ Zhuoyuan Chen
zychen@qdio.ac.cn

[1] Key Laboratory of Marine Environmental Corrosion and Bio-fouling, Institute of Oceanology, Chinese Academy of Sciences, 7 Nanhai Road, Qingdao 266071, China

[2] Center for Ocean Mega-Science, Chinese Academy of Sciences, 7 Nanhai Road, Qingdao 266071, China

[3] Open Studio for Marine Corrosion and Protection, Pilot National Laboratory for Marine Science and Technology (Qingdao), No. 1 Wenhai Road, Qingdao 266237, China

Graphic abstract

WO_3/GO composite exhibits enhanced sustained photoelectrochemical cathodic protection performance for 304 stainless steel under the assistance of TiO_2.

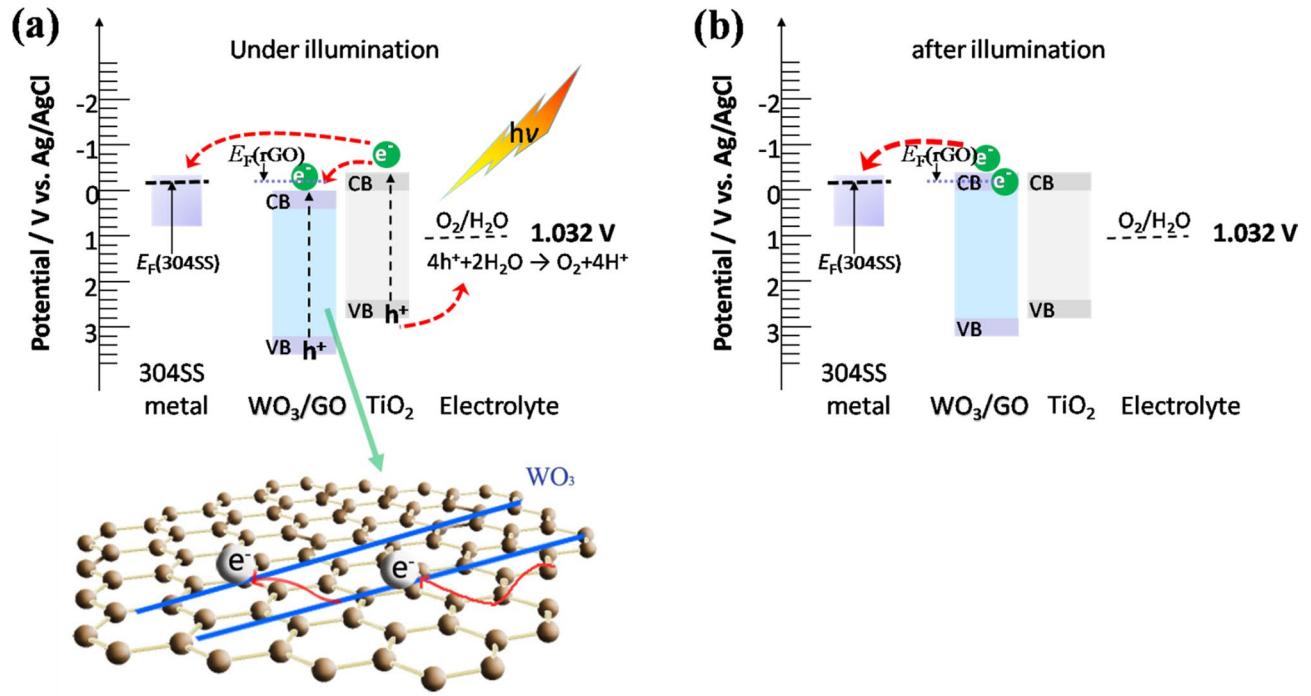

Keywords WO_3 nanothorn clusters · Nanoscale graphene oxide · Composite materials · Electron storage · The sustained photoelectrochemical cathodic protection

1 Introduction

Recently, the photoelectrochemical cathodic protection technology, which utlizes solar energy to generate photoinduced electrons through the semiconductor photoelectric conversion technology to protect metallic structures, has attracted increasing attentions of scientists since it is environmental friendly and sustainable [1–11]. It is not like other corrosion protection technologies, which may consume materials, deplete energy and even pollute the environments. However, this technology has an inherent drawback, that is, needing the light illumination for generating electrons. In the dark, the semiconductor materials will not possess the photoelectrochemical effect, and thus they cannot generate the photoinduced electrons to offer the cathodic protection for the coupled metallic materials. Therefore, studying and developing the electron storage materials, and conjuncting them with semiconductor materials for photoelectrochemical cathodic protection would benefit for solving the above-mentioned issues without sunshine (e.g., at night or in rainy and cloudy days) [12–17]. In the presence of light illumination, some of the photogenerated electrons will transfer to the coupled metallic materials and provide the photoelectrochemical cathodic protection for them, meanwhile, the excess photogenerated electrons can be stored by the electron storage materials. The stored electrons can be released and transferred to the coupled metallic materials to keep the cathodic protection running effectively once the light is shut off, which is called the sustained photoelectrochemical cathodic protection.

In the last 20 years, WO_3, as a kind of electron storage material, shows potential application in photochromism, photoelectrochemical storage and sustained photoelectrochemical cathodic protection for metallic materials [18–24]. The ability of the photoinduced reduction energy storage of WO_3 is achieved by the injection and extraction of electrons and H^+ or Li^+ cations, and consequently resulting in the color change. The intensity of energy storage and the switching time of the color change in WO_3 strongly rely on the availability of electrons for facilitating the redox reaction of $W^{6+} \leftrightarrow W^{5+}$. When electrons and cations are injected, the electronic structure of WO_3 is modified, and the Fermi level of WO_3 moves upward (i.e., shift negatively). As a result, excess electrons fill the t_{2g} band of WO_3, which is

accompanied with the color change of tungsten from transparent to blue. WO_3 has been applied in the sustained photoelectrochemical cathodic protection for metallic materials. Tatsuma et al. reported that a composite of TiO_2 coating layer coupled with a WO_3 coating layer, in which can store the electrons and reductive energy like a pool [12]. 304 SS can be protected from corrosion under UV illumination with TiO_2 and WO_3 coating (50 % area of each single coating), which exhibits sustained photoelectrochemical cathodic protection effect because the stored charge is retained for approximately 4 h after shutting off the UV illumination. The TiO_2/WO_3 composite coating has also the identical function but the efficiency is lower than the composite coated separately with TiO_2 and WO_3 (50 % area of each single coating). Zhou et al. prepared TiO_2/WO_3 bilayer coatings on 304 SS [13], and the 304 SS can maintain the effect of sustained photoelectrochemical cathodic protection for 6 h in the dark after 1 h of illumination by UV light. The effective modifications are essential to further harness and enhance the energy storage property of WO_3.

Since the emergence of graphene in 2004 [25], enormous studies have proved that graphene, with the distinctive quasi-two-dimensional (2D) structure of individual graphene sheets, has a monolayer of sp^2-bonded carbon atoms. Graphene exhibits extraordinary electronic transport properties and physicochemical properties [26, 27]. Reduced graphene oxide (rGO) has been proved that it can assist the transfer of the electrons when incorporating rGO with WO_3 nanoparticles [28, 29]. And the graphene oxide (GO) sheets, adopted as the supporters, can anchor WO_3 to grow on them during the synthesis process, and thus, the electrons can be transferred via the 2D GO sheets and stored in the adjacent WO_3 nanoparticles. This kind of GO-based composite is expected to improve the electron storage ability of WO_3. Nevertheless, preparation of such composite requires that the WO_3 is compatible with GO and is homogeneously distributed. The oxygen-containing functional groups in GO make them as desirable supporters to anchor components for the synthesis of GO-based composites. The graphene-based nanocomposites are usually prepared from the reduction of GO-based materials through a chemical method or heat treatment. However, these methods have some defects, i.e., using toxic hydrazine hydrate, suffering from some harsh conditions including using organic solvents, poisonous agents, and heat treatment processes.

In the present paper, the WO_3/GO nanothorn cluster composites were synthesized using nanoscale graphene oxide and WCl_6, and using a facile solovthermal in situ growth method in alcohol. During the solvothermal process, the growth of WO_3 on GO sheets and partial reduction of GO occurred simultaneously, resulting in the uniform deposition of minor scale WO_3 nanothorns on the partially reduced GO (PRGO) nanosheets. Finally, the application of WO_3/GO composite in the sustained photoelectrochemical cathodic protection after shutting off the light was investigated. Combining the prepared WO_3/GO composite with a semiconductor material, the photoinduced electrons generated by the selected semiconductor material can be used to charge the WO_3/GO composite. In this work, the commercial TiO_2 (P25) without any pre-treatment was chosen as the semiconductor, and the photoelectrode was fabricated by coating TiO_2 and the WO_3/GO composite on the surface of the FTO conductive glass (single coating layer, 50 % area of each material). Using this coating method, the electron storage efficiency of the WO_3/GO–TiO_2 system will be greatly improved compared with other coating methods [12]. The untreated commercial TiO_2 will charge the WO_3/GO composite using the photoinduced electrons generated by TiO_2. Subsequently, utilizing the WO_3/GO–TiO_2 system, the photoelectrochemical cathodic protection performance and the sustained photoelectrochemical cathodic protection performance after shutting off the light for 304 SS were studied. Compared with that of pure WO_3, the WO_3/GO composite exhibits an enhanced electron storage performance and an enhanced sustained photoelectrochemical cathodic protection performance for the coupled 304 SS under the assistance of TiO_2 after shutting off the light. The promoting mechanism for the enhanced electron storage performance of the WO_3/GO system was also studied in this work. The effect of GO or rGO on the electron storage property of the prepared WO_3/GO composites in the sustained photoelectrochemical cathodic protection for metallic materials was analyzed. This work would be helpful for controlling the growth and the electronic storage property of WO_3, meanwhile, it would also benefit the development of the sustained photoelectrochemical cathodic protection technique for metals coated with photoelectric energy storage materials.

2 Experimental

2.1 Preparation of the WO_3/GO composite and fabrication of the WO_3/GO–TiO_2 photoelectrode

The preparation of the WO_3/GO composite was based on a facile method that combines the solovthermal method [30] with the in-situ growth method. The preparation process is illustrated in Scheme 1. First, the GO, produced from natural graphite, was obtained as exfoliated powder from JCnano (JCGO-99-1-50n, the size of the GO sheet is approximately 50 nm). A calculated amount of GO was added into ethanol and ultrasonically vibrated for 2 h to form a stable dispersion with a concentration of 0.5 mg mL^{-1}. The detailed preparation process is listed as follows: A certain amount of the prepared GO dispersion, which was accounted for

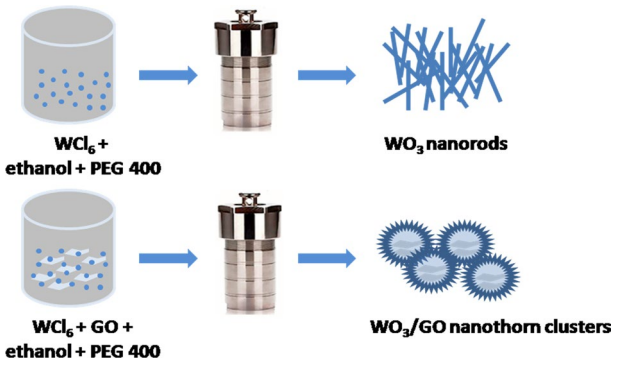

Scheme 1 Schematic illustration for the synthesis procedure of the pure WO_3 and the WO_3/GO composites

0.1, 0.2, 0.3 and 0.4 wt% of the mass of WO_3, were dissolved in 20 mL of ethanol, ultrasonically dispersed for 1 h. WCl_6 (0.4 g) were dissolved in a mixture of ethanol (40 mL) and poly(ethylene glycol) (20 mL, molecular weight M_W = 400 Da) under magnetic stirring. The resulting solution was poured into the GO solution under magnetic stirring to form a homogeneous solution, which was then transferred to a Teflon-lined stainless steel autoclave and heated at 180 °C for 24 h. A blue precipitate was collected by centrifugation and washed with ethanol for several times, and the WO_3/GO composite was obtained after drying at 60 °C. The WO_3/GO composites with the GO accounting for 0.1, 0.2, 0.3 and 0.4 wt% of the mass of WO_3 are denoted as WO_3/GO 0.1, WO_3/GO 0.2, WO_3/GO 0.3 and WO_3/GO 0.4, respectively. For comparison, the pure WO_3 was also prepared by the same method without adding GO. It should be claimed that the "WO_3" written in this paper is actually nonstoichiometric. Here, the "WO_3" is used to describe the products just to keep consistency throughout the whole paper for readability.

The WO_3/GO–TiO_2 system thin-film photoelectrodes were fabricated by evenly depositing the TiO_2 (P25) and the prepared WO_3/GO powder slurry separately onto the surface of the fluorine-doped tin oxide (FTO) conductive glass. Commercialized FTO conductive glass was used in this work and the FTO conductive glass was 40×10 mm^2 in size. Prior to the deposition, the FTO glass was ultrasonically cleaned in acetone of analytical grade for 5 min, rinsed with deionized water, and then dried with a clean dry airflow. One edge of the conductive side of the FTO glass was carefully covered with insulating tapes, leaving an exposed surface of 20×10 mm^2, which was divided into two equal parts of 10×10 mm^2, respectively. Then, 1 mg of the TiO_2 (P25) and 1 mg of the prepared WO_3 or WO_3/GO powder were respectively mixed with 0.1 mL of deionized water in an agate mortar, and were carefully ground for 10 min to form slurry. The TiO_2 slurry was evenly spread over one half of exposed effective area of the FTO glass, that is 10×10 mm^2, while the other part of the exposed area of the FTO glass was evenly coated with the prepared WO_3 or WO_3/GO slurry. The insulating tape on the edge of the FTO glass was removed after the slurry had dried in ambient air. After that, the FTO glass deposited with the as-prepared powder was heated to 80 °C for 2 h. Uncoated parts of the conductive side of the FTO glass were isolated with insulating glue. Besides, the WO_3/GO electrode, pure WO_3 electrode or pure TiO_2 (P25) electrode were also fabricated by uniformly depositing 1 mg of the WO_3/GO composite, pure WO_3, or pure TiO_2 (P25) slurry onto the exposed effective area (10×10 mm^2) of the FTO glass.

The 304 SS electrode was prepared by embedding a square 304 SS in epoxy resin and the exposed area for testing was 10×10 mm^2. The 304 SS electrode was successively wet ground to 2000 grits by SiC papers before being ultrasonically cleaned in analytical grade ethanol for 5 min.

2.2 Characterizations

The crystalline structures of the prepared powders were identified using Ultima IV X-Ray Diffractometer (XRD) (Rigaku Co., Tokyo, Japan). The morphologies and the microstructure of the prepared powders were analyzed using a scanning electron microscope (SEM) (F250, FEI Company, USA) and a high-resolution transmission electron microscope (HRTEM) (Tecnai G20, FEI Company, USA). The elemental composition and the bonding information of the synthetic products were analyzed using an X-ray photoelectron spectroscopy (XPS) on a Thermo VG scientific spectrometer; model ESCALAB 250 (Al Kα, $h\nu = 1486.6$ eV; Mono X-ray source). The binding energy was calibrated according to the signal of adventitious carbon (binding energy = 284.8 eV). The Raman spectra were recorded on an inVia spectrometer (Renishaw, England) with a laser excitation of 633 nm.

2.3 Electrochemical/photoelectrochemical measurements

The electrochemical performance of the WO_3/GO electrode or pure WO_3 electrode (working electrode) were examined by measuring the electrochemical impedance spectra (EIS). The WO_3/GO or pure WO_3 thin-film photoelectrode was acted as the working electrode. A Pt electrode served as the counter electrode and the reference electrode was the Ag/AgCl electrode. EIS tests were performed in 0.1 M Na_2SO_4 in the dark at open circuit potential over the frequency range between 10^5 and 10^{-1} Hz, with a 5 mV AC perturbation using 12 points/decade.

The photoelectrochemical cathodic protection and sustained photoelectrochemical cathodic protection performances were evaluated by the variations of the current

densities of the galvanic couple between the 304 SS electrode and the prepared photoelectrode and the variations of the potentials of the 304 SS electrode coupled with the prepared photoelectrode under intermittent white light on and off. These measurements were performed in 3.5 wt% NaCl solution using a CHI 660D electrochemical work station (Shanghai Chenhua Instrument Co., Ltd.), which is similar to the arrangement that has been used previously [31]. The white light source was a 300-W Xe arc lamp (PLS-SXE300C, Beijing bofeilai Co. Ltd., Beijing, China). The light passed through a flat circular quartz window and illuminated on the photoelectrode. The light intensity was approximately 520 mW cm^{-2} at the sample surface.

3 Results and discussion

3.1 Morphology, microstructure and composition analyses of the prepared WO_3/GO composites

The crystal structures of the prepared WO_3/GO composites were characterized using XRD and the results are shown in Fig. 1. The XRD patterns of the GO and the prepared pure WO_3 are also given in Fig. 1 for comparison. All diffraction peaks of pure WO_3 match well with the hexagonal WO_3 phase (JCPDF card no: 85-2460) [32, 33]. The diffraction peak of (002) of WO_3 phase (JCPDF card no: 85-2460) in the WO_3/GO 0.1 composite shifts towards higher angles compared with that of pure WO_3, indicating the slight lattice contraction of WO_3. When the amount of GO increases to 0.2 and 0.3 wt%, the diffraction peaks of the WO_3/GO 0.2 and WO_3/GO 0.3 composites correspond to another hexagonal WO_3 phase (PDF#33-1387), implying

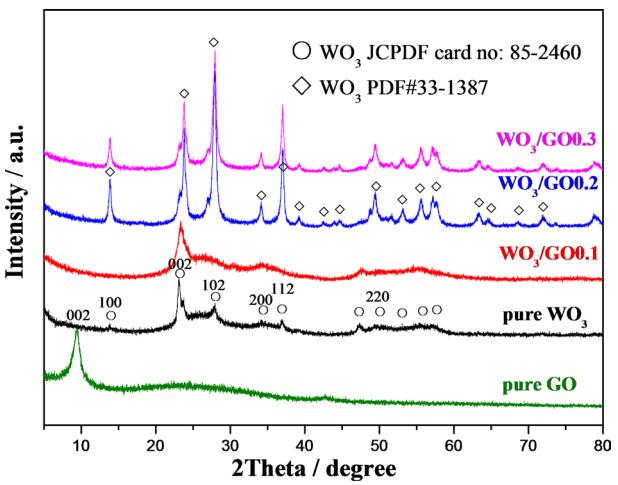

Fig. 1 XRD patterns of the prepared pure GO, pure WO_3 and WO_3/GO composites

a gradual change of the crystal phase of WO_3. These results reveal that the addition of nanoscale GO sheets during the solvothermal synthesis of WO_3 could influence the crystal phase by changing the crystallization behaviors and kinetics of WO_3. The added GO possesses oxygen-containing functional groups on its surface, which greatly enhances the interaction between the outermost oxygen of WO_3 and the oxygen functional groups on the surface of GO [34, 35], and consequently influences the lattice and crystallinity of WO_3 as mentioned in literatures [34–36]. As compared the crystallization of the WO_3/GO composites with pure WO_3, the GO as a template in the solvent will strengthen the reactions among the components or ions. The addition of GO is beneficial for anchoring the components or ions to combine and react on the surface of GO, which promotes the synthesis and the crystallization of the composite. Besides, as shown from the XRD pattern of pure GO, the diffraction peak of (002) for GO located at 10.2° is not a sharp peak, which locates at a lower peak position by comparing with those at 10.8° for the GO in some literatures [34, 37]. The diffraction peak of the XRD pattern of GO is in terms of its interlayer spacing, relating to the sheet size and the degree of oxidation. The smaller sheet size of nanoscale GO will lead to the less overlap of the sheet, and then lead to the less sharp of the diffraction peak at 10.2°. The higher oxidation degree of GO will bring in more interlayer groups, enlarge the interlayer spacing and cause the shift of the diffraction peak towards the lower peak position. Therefore, this result confirms that the GO used in this work are nanoscale sheets with a high oxidation degree and a large amount of groups (such as oxygen-containing groups) in the interlayers of the GO. This characteristic will influence the growth of WO_3. In addition, the diffraction peak of (002) of the adopted GO at 10.2° is not observed in the WO_3/GO film that may due to the low content of GO in it.

SEM and HRTEM were carried out to study the morphologies of the prepared WO_3/GO 0.2 and pure WO_3. Figure 2 shows the SEM images of the prepared pure WO_3 at low (Fig. 2a) and high (Fig. 2b) magnifications. The pure WO_3 sample exhibits nanorods (NRs) structure with the diameter of approximately 33–47 nm and the length of approximately 190 nm. During the synthesis of WO_3, the sulfate ions will be adsorbed on the crystal faces paralleled to the c-axis of WO_3 to form WO_3 NRs [32]. Figure 3 shows the SEM image, TEM images and HRTEM images of the prepared WO_3/GO 0.2 composite. The results suggest that the WO_3/GO composite grow in the form of nanothorn clusters. The high-magnification TEM images and the HRTEM images of the WO_3/GO 0.2 composite confirm that the WO_3 NRs were refined and agglomerated to form nanothorn clusters compared with the pure WO_3. In Fig. 3e, it can be seen that the WO_3 were anchored growing on GO slice layer. The diameter and length of an

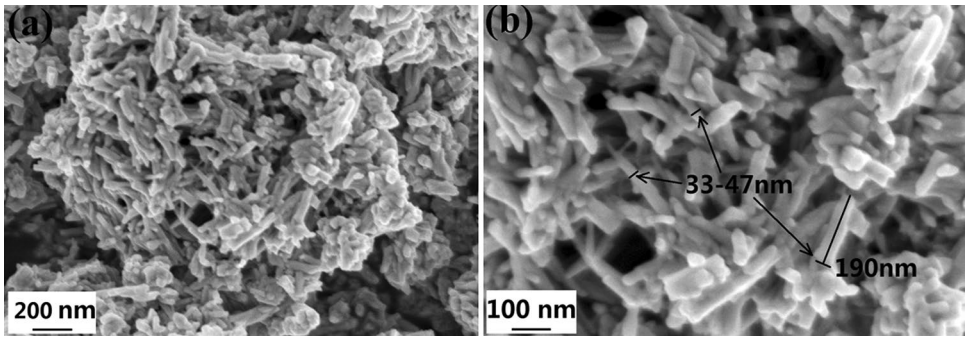

Fig. 2 **a** The low-magnification SEM image and **b** the high-magnification SEM image of the prepared pure WO_3

individual WO_3 nanothorn in the WO_3/GO 0.2 composite are approximately 4.8 nm and 70 nm, respectively, which are much smaller than those of the pure WO_3. In Fig. 3f, the lattice fringe of 0.632 nm and 0.384 nm can be indexed as the (100) and (002) planes of hexagonal WO_3, respectively [33]. The lattice fringe of 0.384 nm in Fig. 3f indicates that WO_3 grew in parallel along the [002] direction to form nanothorn [38]. GO slice layer not only provides the nucleation sites for the growth of WO_3 grains, but also restrains the growth of the WO_3, resulting in the formation of much shorter WO_3 nanothorn for the WO_3/GO 0.2 composite compared with pure WO_3. During the preparation process, W^{6+} was firstly adsorbed on the surface of GO slice by electrostatic interaction, and then, the WO_3 nanothorns were generated via in-situ condensation and dehydration via the alcoholysis process. The electrostatic adsorption property of GO with oxygen-containing functional groups can induce the WO_3 nanothorns to aggregate in the form of clusters; each cluster comprises many small nanothorns with uniform length and width.

XPS measurements were performed to determine the chemical compositions and the valence states of the components for the prepared WO_3 and WO_3/GO 0.2 composite, and the relevant results are shown in Fig. 4. Figure 4a shows the W4f XPS core level spectra. The binding energy peaks of pure WO_3 locate at 34.4 and 36.5 eV, respectively, which correspond to the typical binding energies of W^{5+} oxidation states. The binding energy peaks of the WO_3/GO 0.2 composite are found at 36.2 and 38.4 eV, which are attributed to the spin-orbit splitting of the W4f components (W4f7/2 and W4f5/2) and are consistent with those of tungsten (VI) [39, 40]. The XPS results indicate that the oxidation state of W in WO_3 transfers from W^{5+} to W^{6+} due to the addition of GO. The oxygen-containing functional groups on the surface of GO contribute to the interaction between WO_3 and GO sheets [41], which may sustain the valence state of W with W^{6+}. Figure 4b shows the C1s XPS core level spectra. The main peak at the binding energy of 284.8 eV is attributed to the non-oxygenated C–C and C=C bonds. The high-resolution C1s XPS spectrum of the WO_3/GO 0.2

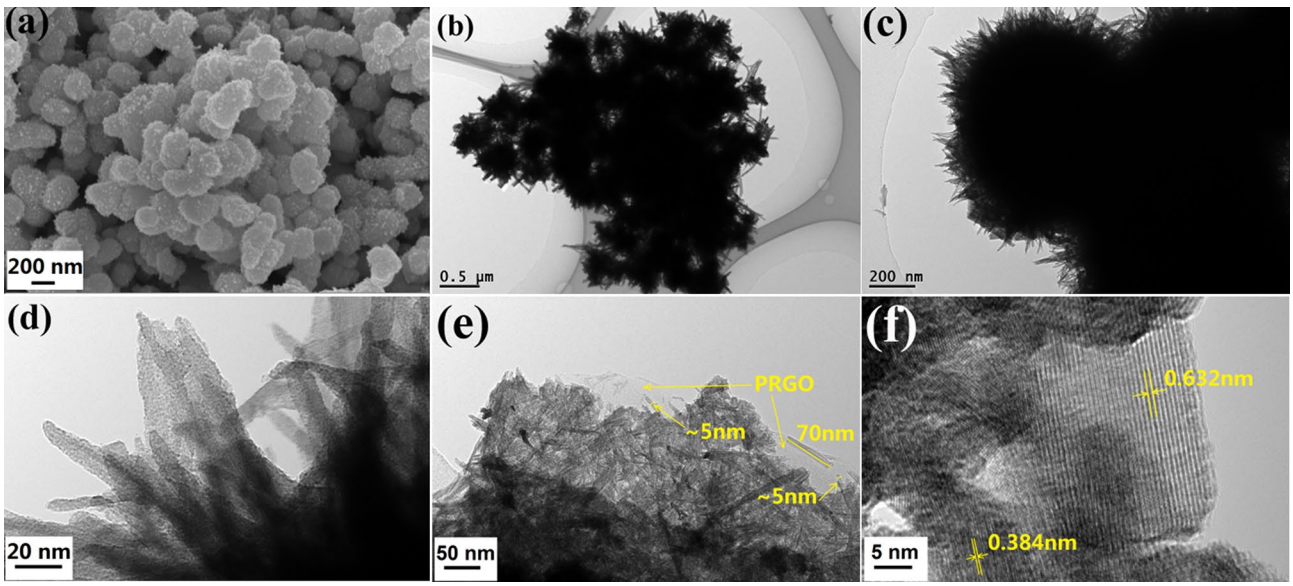

Fig. 3 **a** SEM image, **b**, **c** TEM images and **d**, **e**, **f** HRTEM images of the prepared WO_3/GO 0.2 composite

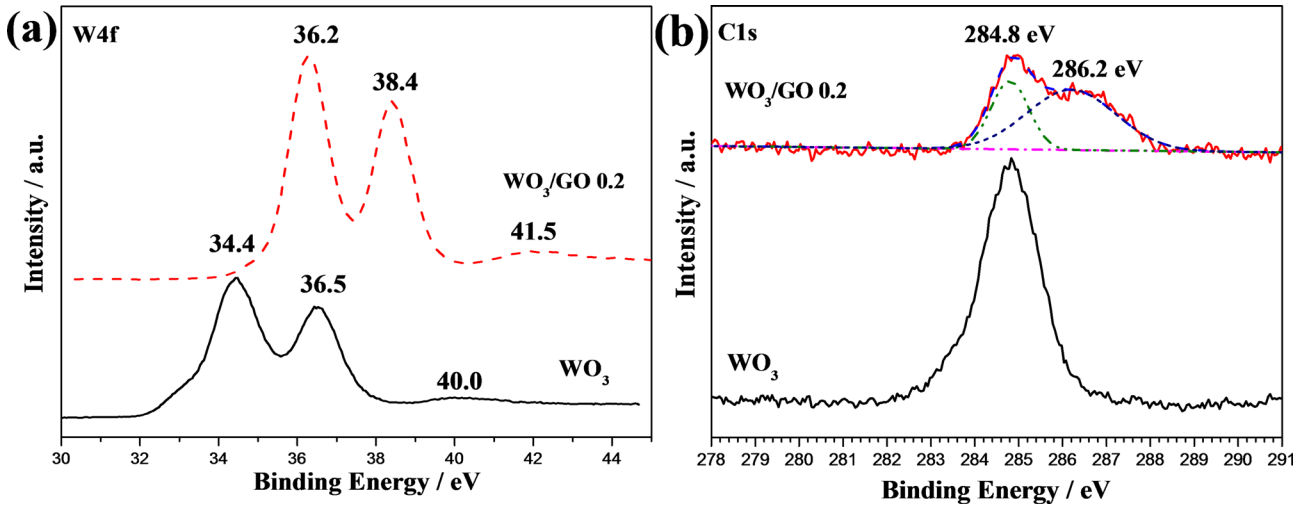

Fig. 4 High-resolution XPS spectra of **a** W4f and **b** C1s for the prepared pure WO_3 and WO_3/GO 0.2 composite

composite can be deconvolved into two peaks corresponding to C atoms in the C–O bonds at 286.2 eV and the C–C bonds at 284.8 eV due to the presence of GO [42, 43]. C peak is not observed at around 281 eV, indicating that the potential carbide species, such as WC, are not presented in the WO_3/GO 0.2 composite [44].

Raman spectroscopy is a useful technique for distinguishing the order structure and the reduction degree of GO layers and GO-based materials [42, 45]. Therefore, the Raman spectra of GO and the prepared WO_3/GO composites were measured and the results are shown in Fig. 5. As expected, the pure GO has two peaks located at around 1351 and 1599 cm^{-1}, corresponding to the D and G peaks of hexagonal carbon-type structure of graphene, respectively. The G band peak at around 1599 cm^{-1} is the characteristic peak of graphitic sheets due to the C–C vibrations of the carbon with a sp^2 orbital structure, while the D band at 1351 cm^{-1} is related to the defects/disorders vibration of the C–C bond [46–48]. Based on the results shown in Fig. 5, the intensity ratios of D peak to G peak, I_D/I_G, for WO_3/GO 0.1, WO_3/GO 0.2 and WO_3/GO 0.3 are 1.51, 1.43 and 1.20, respectively. The higher the value of I_D/I_G is, the higher the reduction degree of GO achieves [42, 45], and thus, the value of I_D/I_G is usually used to evaluate the reduction degree of GO. The values of I_D/I_G in the prepared WO_3/GO 0.1 and WO_3/GO 0.2 composites are higher than that of GO (1.33), revealing that the GO was partly reduced after the solvothermal process during the growth of WO_3. Therefore, the Raman results suggest that the GO has been partially reduced into rGO [34]. The higher reduction degree of GO is beneficial to the charge transfer in the WO_3/GO composite. When the amount of GO increases to 0.3 wt%, the I_D/I_G (1.20) are lower than that of the untreated GO. This may be due to the excessive addition of GO, which induces the agglomeration and accumulation of GO in the composite.

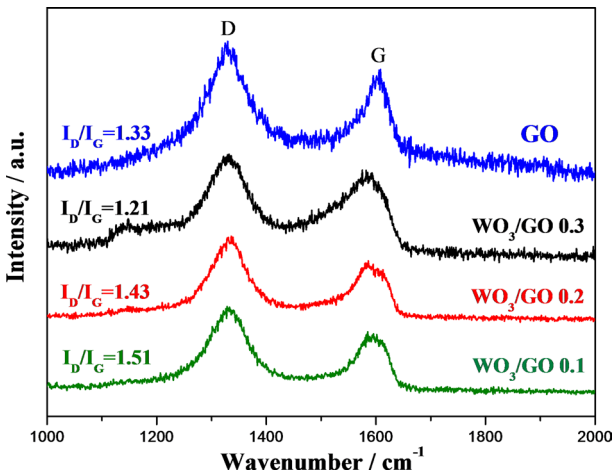

Fig. 5 Raman spectra of the prepared WO_3/GO composites and pure GO

3.2 The sustained photoelectrochemical cathodic protection performance of the prepared WO_3/GO–TiO_2 system

Firstly, in order to analyze the effect of GO on the electrical properties of WO_3, the EIS plots of the WO_3 and WO_3/GO 0.2 thin-film photoelectrodes were measured in 0.1 M Na_2SO_4 and the results are shown in Fig. 6. The equivalent electrical circuit employed for fitting the obtained EIS plots was inserted in Fig. 6. In the equivalent circuit, R_s was the solution resistance; Q represents the constant phase angle element, its impedance is equal to $(Y_0(j\omega)^n)^{-1}$, where ω is

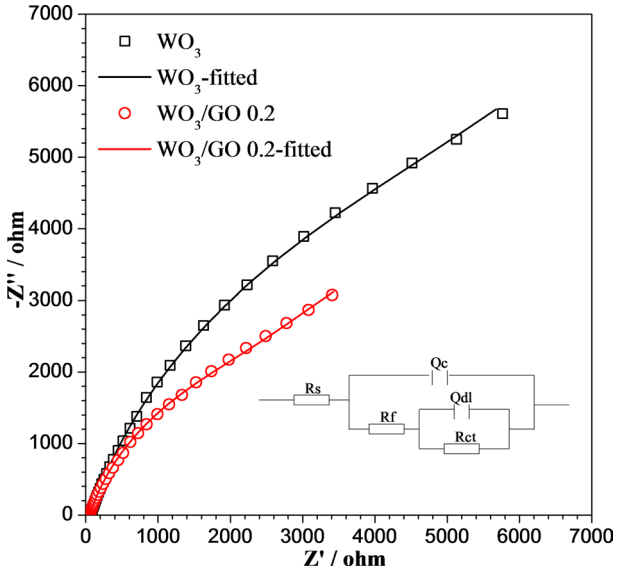

Fig. 6 The EIS plots of the prepared pure WO_3 and WO_3/GO 0.2 photoelectrodes in 0.1 M Na_2SO_4

the ac-voltage angular frequency (rad s^{-1}), and Y_0 and n are the frequency-independent parameters. Q_c and R_f are the capacitance and resistance of the surface film, respectively. Q_{dl} and R_{ct} are the double layer capacitance and the charge transfer resistance of the electrochemical reactions occurred at the film/FTO substrate interface, respectively. As shown in Fig. 6, the measured data are the dots with different symbols, while, the solid lines are the fitted results using the provided equivalent circuit. The measured data are fitted very well. Table 1 shows the fitted parameters of the EIS data. R_f is decreased in the order of $R_f(WO_3/GO\ 0.2) < R_f(WO_3)$, suggesting that the resistance of the WO_3 was decreased after the hybridization with GO. This result reveals that the hybrid structure of WO_3/GO 0.2 facilitates the electron transfer among the charge collector of WO_3, demonstrating that the addition of GO nanosheets enhances the conductivity of the WO_3/GO composites.

The sustained photoelectrochemical cathodic protection performance of a photoelectric conversion energy storage material mainly depends on the ability of supplying electrons to the coupled metals to be protected after the light is shut off. WO_3 majorly acts as an electron storage material. However, single WO_3 cannot offer enough photoinduced electrons to the coupled metals under white light illumination because the conduction band of WO_3 is not more negative enough than the work function of the coupled metals. TiO_2 is a typical semiconductor material with good photoelectrochemical cathodic protection performance and it can offer a lot of electrons to the coupled metals under white light illumination. Unfortunately, it does not possess the electron storage function. Therefore, WO_3 are often adopted to assist TiO_2 for the purpose of achieving the ability for storing up the photoinduced electrons [12, 13].

The cathodic protection current densities of the prepared composite photoelectrodes immersed in 3.5 wt% NaCl for the galvanic coupled 304 SS electrode under intermittent white light illumination are shown in Fig. 7a. The cathodic protection current densities under white light illumination are positive, indicating that the photoinduced electrons generated by the photoelectrodes could transfer to the coupled 304 SS electrode. Thus, the photoelectrochemical cathodic protection derived from the prepared composite photoelectrodes for 304 SS has been achieved due to the reaction of the transferred photogenerated electrons with the dissolved oxygen in NaCl solution on the 304 SS surface. Figure 7b shows the local enlarged drawing of the rectangular area in Fig. 7a, from which it can be clearly observed that the values of the cathodic protection current densities of the prepared photoelectrodes for the galvanic coupled 304 SS electrode after the light was switched off for 100 s in the third cycle of the light on and off. The corresponding values of current density in the third cycle of the light on and off in Fig. 7a after 100-s illumination (I_1) and after the light was switched off for 100 s (I_2) were shown in Table 2. The current densities (I_1) after 100-s illumination of the WO_3–TiO_2–304 SS and WO_3/GO–TiO_2-304 SS systems are lower compared to that of TiO_2-304 SS, which are attributed to the injection of some photoinduced electrons generated by TiO_2 to WO_3 or to WO_3/GO. While, the electrons generated by pure TiO_2 coupled with 304 SS cannot be stored up. Notably, the current densities of the WO_3/GO–TiO_2 system drop much slower comparing to that of pure TiO_2 in the dark when the white light was switched off.

The smaller the current density drop rate after shutting off the light is, the better the sustained photoelectrochemical cathodic protection performance is. As shown in Fig. 7a, b, the current drop rate of the WO_3/GO–TiO_2 system is significantly decreased with the increase of the GO concentration

Table 1 Fitted parameters of the EIS data shown in Fig. 6

	R_s(Ω cm^2)	Q_c		R_f(Ω cm^2)	Q_{dl}		R_{ct}(Ω cm^2)
		(Y_{oc}) (Ω^{-1} cm^{-2} S^{-n})	n_1		(Y_{odl}) (Ω^{-1} cm^{-2} S^{-n})	n_2	
WO_3	62.2	7.69×10^{-5}	0.8027	11,800	2.19×10^{-4}	0.7692	59,910
WO_3/GO	51.84	1.17×10^{-4}	0.803	5703	3.39×10^{-4}	0.955	6519

Table 2 The current densities of the galvanic coupling between the 304 SS electrodes and the prepared photoelectrodes after 100-s illumination (I_1) and the corresponding current densities after the light is switched off for 100 s (I_2) in the third cycle of the light on and off in Fig. 7a

current density / μA cm^{-2}	WO_3–TiO_2-304 SS	WO_3/GO 0.1-TiO_2-304 SS	WO_3/GO 0.2-TiO_2-304 SS	WO_3/GO 0.3-TiO_2 -304 SS	TiO_2-304 SS
I_1	21.01	28.09	25.95	33.2	33.28
I_2	3.58	5.15	5.60	3.42	-3.31

from 0 to 0.2 wt%. However, further increase of the GO mass ratio from 0.2 to 0.3 wt% results in higher current drop rates of the WO_3/GO–TiO_2 system. From the perspective of the sustained photoelectrochemical cathodic protection, high sustained current density after shutting off the light indicates the desirable sustained cathodic protection performance, that is, the larger the value of I_2 in Table 2 is, the better the sustained cathodic protection performance of the system is. When the mass ratio of GO in the WO_3/GO composite is 0.2 wt%, the WO_3/GO–TiO_2 system exhibits the highest sustained galvanic current density (5.60 μA cm^{-2})

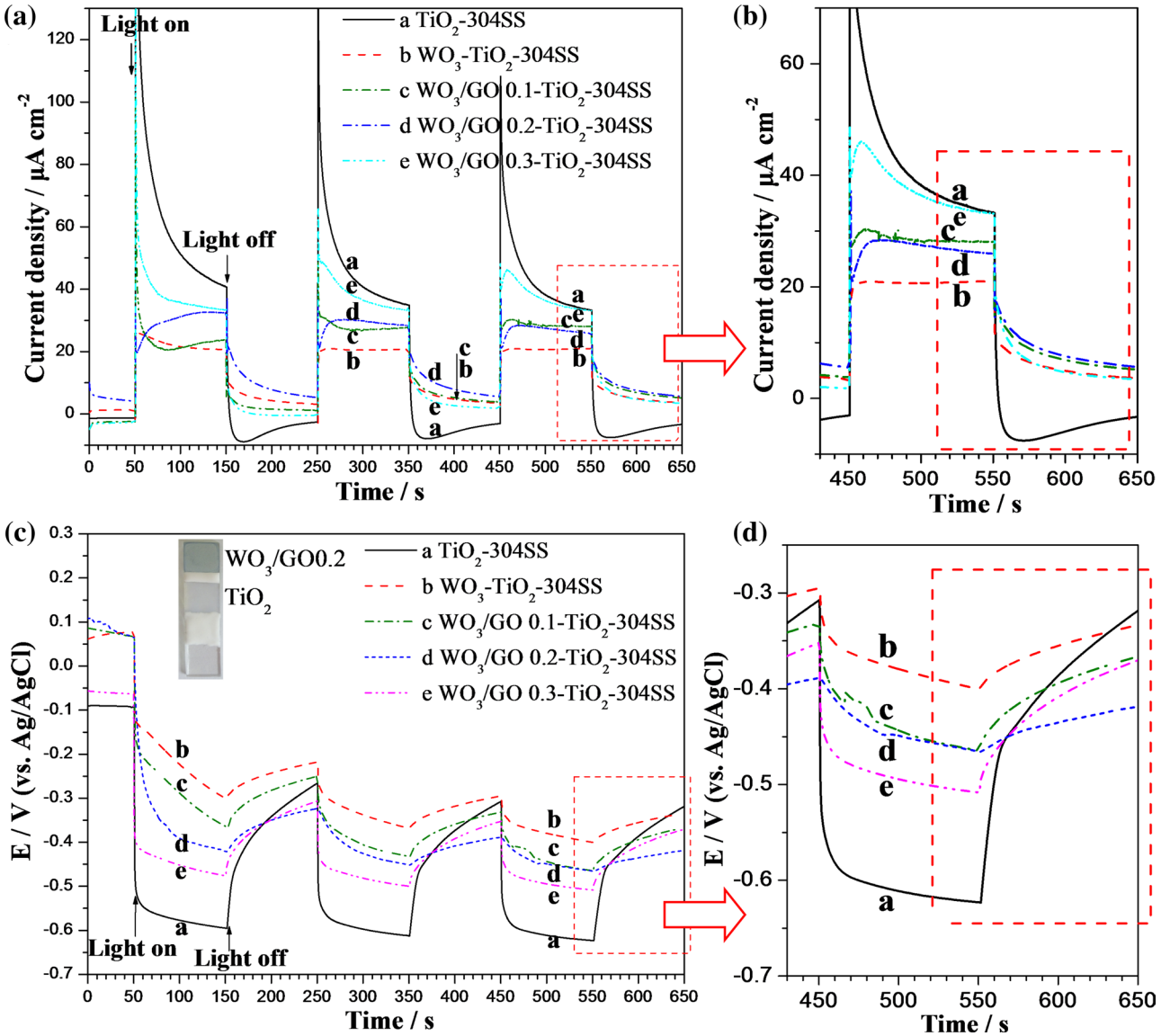

Fig. 7 **a** The photoinduced current densities between the prepared TiO_2, WO_3–TiO_2 or WO_3/GO–TiO_2 thin-film photoelectrode and the 304 SS electrode, **b** the local enlarged drawing of the rectangular area in (**a**); **c** the photoinduced potential variations of the coupled thin-film photoelectrode with the 304 SS electrode under intermittent white light illumination, **d** the local enlarged drawing of the rectangular area in (**c**)

after switching off the light, demonstrating that WO_3/GO 0.2-TiO_2 possesses the optimal sustained photoelectrochemical cathodic protection performance. The hybrid structure in WO_3/GO 0.2-TiO_2 system constructed by WO_3 and GO benefits the transfer and storage of the photoinduced electrons in the WO_3/GO composite.

Figure 7c shows the corresponding variations of the mixed potentials of the 304 SS electrodes coupled with the photoelectrodes under intermittent white light illumination. The mixed potentials of all the coupled electrodes negatively shift immediately once the white light is switched on. When the white light is switched off, the mixed potentials positively shift immediately and gradually move towards their initial values. The negative shift of the mixed potential under white light illumination is caused by the injection of the photoinduced electrons generated by the semiconductor materials into the coupled 304 SS. Figure 7d shows the local enlarged drawing of the rectangular area in Fig. 7c, in which can be clearly depicted the values of the mixed potentials of the galvanic coupling of the 304 SS electrode and the prepared photoelectrodes after the light was switched off for 100 s in the third cycle of the light on and off. The corresponding photoinduced potentials after 100-s illumination (E_1) and the corresponding mixed potentials in the third cycle of the light on and off in Fig. 7c after the light was switched off for 100 s (E_2) were shown in Table 3. Here, the photoinduced potential (E_1) is the value of the galvanic couple between the 304 SS electrode and the photoelectrode after 100-s illumination in the third cycle of the light on and off. In Table 3, although the TiO_2-304 SS coupling shows the most negative photoinduced potential (− 0.62 V), the potentials of TiO_2-304 SS will return to its initial values in the fastest speed after shutting off the light among the couples investigated because of the absence of the electrons storage property of pure TiO_2. In addition, although WO_3–TiO_2 exhibits the lowest returning speed of the mixed potential after shutting off the light, the photoinduced potential of WO_3–TiO_2-304 SS is the smallest (− 0.4 V) under light illumination, which makes it be unacceptable for the application in the field of the photoelectrochemical cathodic protection. The low returning speeds of the mixed potentials of WO_3–TiO_2-304 SS or WO_3/GO–TiO_2-304 SS systems are due to the electron storage property of the WO_3. For the WO_3–TiO_2-304 SS or WO_3/GO–TiO_2-304 SS system under light illumination, some of the photoinduced electrons generated by TiO_2 transfer to the coupled 304 SS, and the excessive photogenerated electrons are injected and stored in the WO_3 or WO_3/GO composite. Simultaneously, W^{6+} is reduced to W^{5+} or W^{4+} by the photoinduced electrons generated by TiO_2, and the Na^+ and H^+ are inserted into WO_3 to form tungsten bronze type structure of H_xWO_3 or Na_xWO_3, resulting in the storage of the photogenerated electrons. When the light is switched off, the stored electrons in tungsten bronze will be released and transferred to the coupled 304 SS, leading to the retarded rise of the mixed potential. Additionally, the electric conductivity of pure WO_3 is relatively low, and the photogenerated electrons cannot efficiently transfer and be stored in it, leading to the generation of the smallest photoinduced potential (− 0.4 V) of the coupling of WO_3–TiO_2-304 SS in the presence of light illumination. Conversely, the WO_3/GO–TiO_2 systems could transfer more photoinduced electrons to WO_3 with the assistance of PRGO and react with the multivalent W ions, resulting in the storage of more photoinduced electrons than that of the WO_3–TiO_2. Therefore, the photoinduced potential of WO_3/GO 0.1-TiO_2-304 SS, WO_3/GO 0.2-TiO_2-304 SS and WO_3/GO 0.3-TiO_2-304 SS are enhanced (more negative) under light illumination compared to WO_3–TiO_2-304 SS (− 0.4 V), as shown in Fig. 7c; Table 3.

After the light is switched off for 100 s in the third cycle of the light on and off, the mixed potential of WO_3/GO 0.2-TiO_2-304 SS (− 0.419 V) is more negative than those of the other systems. According to the photoinduced potential and the potential returning speed after switched off light, WO_3/GO 0.2-TiO_2-304 SS not only shows an enhanced photoinduced potential (− 0.465 V) under light illumination, but also performs a lower returning speed after shutting off the light compared with those of other systems. Therefore, the WO_3/GO 0.2 composite offers an optimal sustained photoelectrochemical cathodic protection for 304 SS after shutting off the white light. The synergistic action for electrons storage in WO_3/GO 0.2 hybrid composite will come up to an optimal extent with the ratio of 0.2 wt% GO. With respect to the further increase of the GO mass ratio to 0.3 wt%, the returning speed of the mixed potential of the WO_3/GO 0.3-TiO_2-304 SS becomes faster than that of the WO_3/GO

Table 3 The photoinduced potentials of the galvanic couple of the 304 SS electrode and the photoelectrode after 100-s illumination (E_1), and the corresponding mixed potentials after the light is switched off for 100 s (E_2) in the third cycle of the light on and off in Fig. 7c

Potential/V (vs. Ag/AgCl)	WO_3–TiO_2-304 SS	WO_3/GO 0.1-TiO_2-304 SS	WO_3/GO 0.2-TiO_2-304 SS	WO_3/GO 0.3-TiO_2-304 SS	TiO_2-304 SS
E_1	− 0.4	− 0.465	− 0.465	− 0.508	− 0.620
E_2	− 0.333	− 0.366	− 0.419	− 0.370	− 0.319

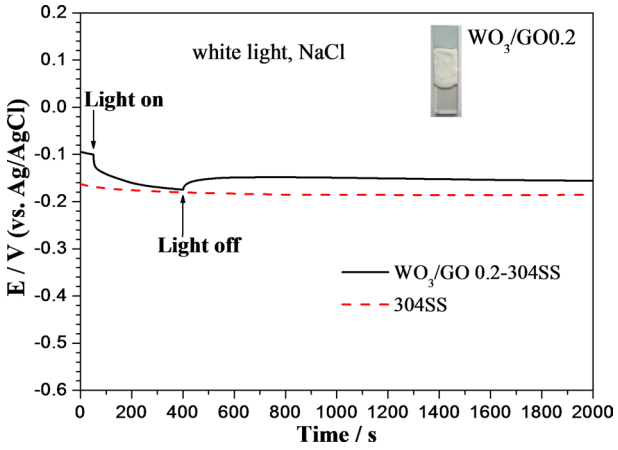

Fig. 8 Variations in the mixed potentials of the 304 SS electrode coupled with the single WO_3/GO 0.2 photoelectrode as well as the potentials of the 304 SS electrode without protection under initially 350-s illumination by white light and subsequently > 2000s in the dark

0.2-TiO_2-304 SS. This is caused by the high electron transport characteristic of partly reduced GO, and the excessive GO will accelerate the release of electrons in WO_3 in the dark, which is unexpected.

Besides, the variations in the mixed potential of the 304 SS electrode coupled with the single WO_3/GO 0.2 photoelectrode (i.e., WO_3/GO 0.2–304 SS) under initial 350-s illumination by white light and subsequently > 2000s in the dark was also measured and the results are shown in Fig. 8. The single WO_3/GO 0.2 can only offer 74 mV photoinduced potential drop for the coupled 304 SS electrode under white light illumination because it cannot charge itself efficiently without the aid of TiO_2. Thus, the single WO_3/GO 0.2 cannot offer an efficient photoinduced cathodic protection and sustained cathodic protection for 304 SS in 3.5 % NaCl under and after white light illumination. In addition, the open circuit potential of 304 SS in 3.5 % NaCl was also given in Fig. 8 for comparison, which is stabilized at − 0.187 V vs. Ag/AgCl.

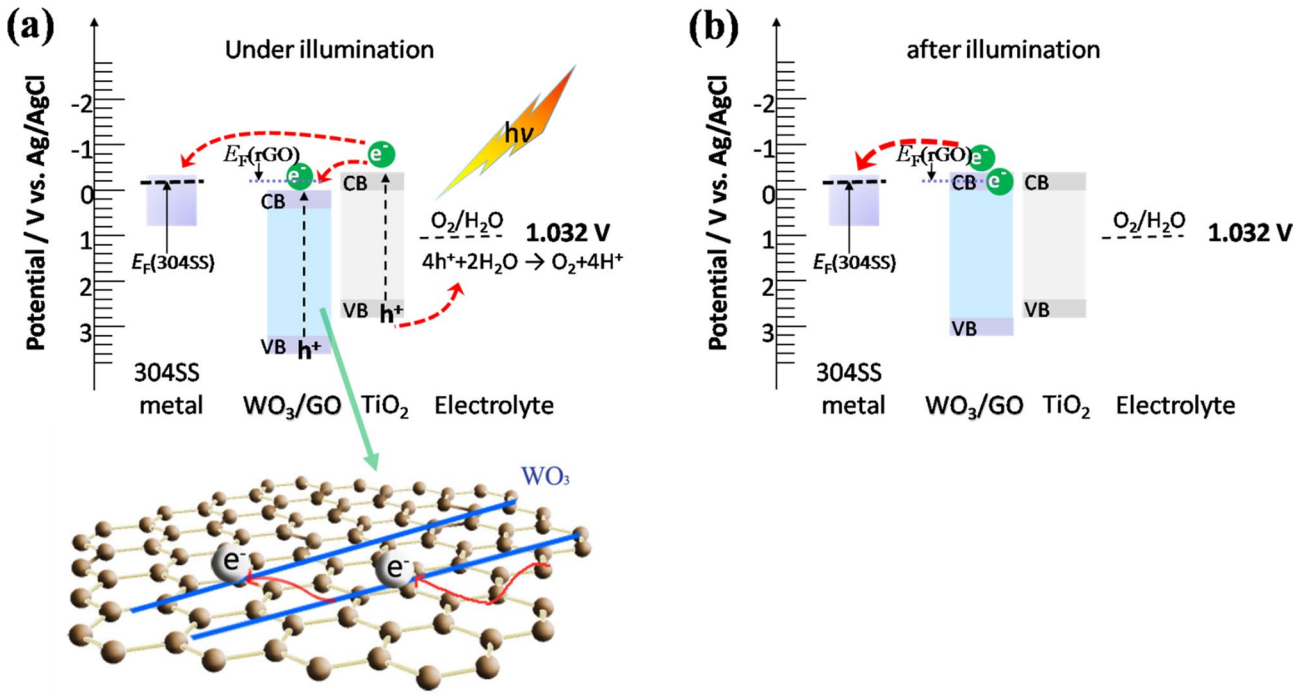

Fig. 9 Proposed mechanism of the enhanced sustained photoelectrochemical cathodic protection performance of WO_3/GO 0.2-TiO_2 for 304 SS. The left part **a** shows the photoelectrochemical cathodic protection of WO_3/GO 0.2-TiO_2 for 304 SS under white light illumination. The right part **b** shows the sustained protection of WO_3/GO 0.2-TiO_2 for 304 SS after shutting off the white light illumination. (E_{CB} for WO_3 = 0.543 V vs. Ag/AgCl. E_{VB} for WO_3 = 3.243 V vs. Ag/AgCl. Redox potential for O_2/H_2O is 1.032 V vs. Ag/AgCl. The Fermi level of 304 SS is approximately − 0.1 V vs. Ag/AgCl.)

3.3 Promotion mechanism of the sustained photoelectrochemical cathodic protection performance of the WO_3/GO 0.2-TiO_2 system after light illumination

Figure 9 illustrates the proposed mechanism for interpreting the enhanced electron storage performance and sustained photoelectrochemical cathodic protection performance of the WO_3/GO 0.2-TiO_2 system. Under white light illumination, the electrons in the valence band of TiO_2 are excited to its conduction band and the photoinduced electrons are generated. Meanwhile, the electrons in the valence band of WO_3 are also excited to its conduction band to generate the photoinduced electrons. Since the Fermi levels of WO_3 and 304 SS are more positive than the quasi-Fermi level of the photogenerated electrons on TiO_2, some of the photogenerated electrons will transfer to the coupled 304 SS electrode and offer the photoelectrochemical cathodic protection for it. The excess photogenerated electrons will transfer to WO_3 and be stored in it. Simultaneously, the Fermi level of WO_3 moves upward (i.e., shift negatively). The remaining holes will be captured by H_2O in the surrounding electrolyte to generate O_2. More importantly, according to the SEM results, WO_3 NRs have been shortened to form nanothorn clusters after the addition of GO. The nanothorn cluster structure increases the contact areas of WO_3 with charges, as well as facilitates electrolyte to diffuse into the inner of WO_3, and thus promotes the charging reaction in WO_3. As illustrated in Fig. 9, the photogenerated electrons will transfer to WO_3/GO 0.2 to achieve the charging reaction. The refinement of WO_3 for WO_3/GO 0.2 hybrid structure provides more storage spaces for the electrons, and ensures that a larger amount of photogenerated electrons are stored in the WO_3/GO 0.2 hybrid composite under light illumination. Then the Fermi level of WO_3/GO 0.2 moves to the more negative potential compared to that of WO_3. Ultimately, this enhances the sustained releasing electrons performance for a long time in the dark. The stored photogenerated electrons in WO_3/GO 0.2 will be released to provide the sustained photoelectrochemical cathodic protection for the coupled 304 SS once shutting off the light.

4 Conclusions

In the present paper, the role of nanoscale GO on the growth and the electron storage performance of WO_3 was studied. With the addition of nanoscale GO, the lattice of WO_3 contracted slightly and the crystallinity of WO_3 was enhanced. The WO_3 nanothorn clusters were formed in the WO_3/GO composite when the GO adding amount is 0.2 wt%. The SEM and HRTEM results indicate that the growth of WO_3 will be anchored on the GO sheets and leads to the formation of nanothorn clusters for the WO_3/GO 0.2 composite compared with pure WO_3. Then, the WO_3 in the WO_3/GO 0.2 composite are refined and grow in the form of nanothorn clusters. The refinement of WO_3 provides more contact areas and more storage spaces for the photogenerated electrons, ensuring a larger amount of the electrons are stored in the WO_3. Besides, the formed hybrid structure of the WO_3/GO composite promotes the transfer and storage efficiency of the electrons in the WO_3/GO 0.2 composite. When WO_3/GO 0.2 was coupled with TiO_2, the WO_3/GO 0.2-TiO_2 system exhibited an enhanced sustained photoelectrochemical cathodic protection performance for the coupled 304 SS after shutting off the white light. More photogenerated electrons formed on TiO_2 can be stored in the WO_3/GO 0.2 composite under the white light illumination, and then continue to inject to the coupled 304 SS electrode after shutting off the white light. The WO_3/GO 0.2 composite is a promising material for the application in the field of sustained photoelectrochemical cathodic protection for metals.

Acknowledgements This work was financially supported by the National Natural Science Foundation of China (Grant Nos. 41976036, 41676069, 41906034), and Key Research and Development Program of Shandong Province (Grant Nos. 2019GHY112085, 2019GHY112066).

References

1. Cui S, Yin X, Yu Q, Liu Y, Wang D, Feng Z (2015) Polypyrrole nanowire/TiO_2 nanotube nanocomposites as photoanodes for photocathodic protection of Ti substrate and 304 stainless steel under visible light. Corros Sci 98:471–477
2. Li H, Wang X, Zhang L, Hou B (2015) Preparation and photocathodic protection performance of CdSe/reduced graphene oxide/TiO_2 composite. Corros Sci 94:342–349
3. Jiang X, Sun M, Chen Z, Jing J, Feng C (2020) High-efficiency photoelectrochemical cathodic protection performance of the TiO_2/$AgInSe_2$/In_2Se_3 multijunction nanosheet array. Corros Sci 176:108901
4. Zhu Y, Xu L, Hu J, Zhang J, Du R, Lin C (2014) Fabrication of heterostructured $SrTiO_3$/TiO_2 nanotube array films and their use in photocathodic protection of stainless steel. Electrochim Acta 121:361–368
5. Lei C, Zhou H, Wang C, Feng Z (2013) Self-assembly of ordered mesoporous TiO_2 thin films as photoanodes for cathodic protection of stainless steel. Electrochim Acta 87:245–249
6. Liu W, Wang Y, Su G, Cao L, Sun M, Guo X, Xu H, Duan R (2012) The effect of incorporating carbon nanotubes in titania films used for the photocathode protection of 304 stainless steel. Carbon 50:3641–3648
7. Sun W, Cui S, Wei N, Chen S, Liu Y, Wang D (2018) Hierarchical WO_3/TiO_2 nanotube nanocomposites for efficient photocathodic protection of 304 stainless steel under visible light. J Alloys Compd 749:741–749

8. Momeni MM, Mahvari M, Ghayeb Y (2019) Photoelectrochemical properties of iron-cobalt $WTiO_2$ nanotube photoanodes for water splitting and photocathodic protection of stainless steel. J Electroanal Chem 832:7–23
9. Guan Z, Wang H, Wang X, Hu J, Du R (2018) Fabrication of heterostructured β-Bi_2O_3–TiO_2 nanotube array composite film for photoelectrochemical cathodic protection applications. Corros Sci 136:60–69
10. Yang Y, Cheng YF (2018) One-step facile preparation of ZnO nanorods as high-performance photoanodes for photoelectrochemical cathodic protection. Electrochim Acta 276:311–318
11. Liu Q, Hu J, Liang Y, Guan ZC, Zhang H, Wang HP, Du RG (2016) Preparation of MoO_3/TiO_2 composite films and their application in photoelectrochemical anticorrosion. J Electrochem Soc 163:C539–C544
12. Tatsuma T, Saitoh S, Ohko Y, Fujishima A (2001) TiO_2-WO_3 photoelectrochemical anticorrosion system with an energy storage ability. Chem Mater 13:2838–2842
13. Zhou M, Zeng Z, Zhong L (2009) Photogenerated cathode protection properties of nano-sized TiO_2/WO_3 coating. Corros Sci 51:1386–1391
14. Zhu Y, Du R, Chen W, Qi H, Lin C (2010) Photocathodic protection properties of three-dimensional titanate nanowire network films prepared by a combined sol–gel and hydrothermal method. Electrochem Commun 12:1626–1629
15. Li H, Wang X, Liu Y, Hou B (2014) Ag and SnO_2 co-sensitized TiO_2 photoanodes for protection of 304SS under visible light. Corros Sci 82:145–153
16. Yang J, Wang X, Yang X, Li J, Zhang X, Zhao J (2015) Energy storage ability and anti-corrosion properties of Bi-doped TiO_2 nanotube arrays. Electrochim Acta 169:227–232
17. Liang Y, Guan ZC, Wang HP, Du RG (2017) Enhanced photoelectrochemical anticorrosion performance of WO_3/TiO_2 nanotube composite films formed by anodization and electrodeposition. Electrochem Commun 77:120–123
18. Bechinger C, Ferrer S, Zaban A, Sprague J, Gregg BA (1996) Photoelectrochromic windows and displays. Nature 383:608–610
19. Lee SH, Deshpande R, Parilla PA, Jones KM, To B, Mahan AH, Dillon AC (2006) Crystalline WO_3 nanoparticles for highly improved electrochromic applications. Adv Mater 18:763–766
20. Long M, Tan B, Hu P, Zhou B, Zhou Y (2015) Scalable one-step synthesis of TiO_2/WO_3 films on titanium plates with an efficient electron storage ability. J Mater Chem A 3:10195–10198
21. Xiao Y, Yu Y, Zhang W (2018) Composite structures for enhanced photoelectrochemical activity: WS_2 quantum dots with oriented WO_3 arrays. J Mater Sci 53:10338–10350
22. Vujković M, Nedić Z, Tančić P, Aleksić OS, Nikolić MV, Mioč U, Mentus S (2016) Electrochemical lithiation/delithiation kinetics and capacity of phosphate tungsten bronze and its chemically pre-lithiated derivatives in aqueous solutions. J Mater Sci 51:2481–2489
23. Yang Y, Cheng YF (2020) Visible light illuminated high-performance WO_3–TiO_2–$BiVO_4$ nanocomposite photoanodes capable of energy self-storage for photo-induced cathodic protection. Corros Sci 164:108333
24. Guan ZC, Wang X, Jin P, Tang YY, Wang HP, Song GL, Du RG (2018) Enhanced photoelectrochemical performances of ZnS–Bi_2S_3/TiO_2/WO_3 composite film for photocathodic protection. Corros Sci 143:31–38
25. Novoselov KS, Geim AK, Morozov SV, Jiang D, Zhang Y, Dubonos SV, Grigorieva IV, Firsov AA (2004) Electric field effect in atomically thin carbon films. Science 306:666–669
26. Huang X, Qi X, Boey F, Zhang H (2012) Graphene-based composites. Chem Soc Rev 41:666–686
27. Li M, Ji X, Cui L, Liu J (2017) In situ preparation of graphene/polypyrrole nanocomposite via electrochemical co-deposition methodology for anti-corrosion application. J Mater Sci 52:1–15
28. Guo J, Li Y, Zhu S, Chen Z, Liu Q, Zhang D, Moon W, Song D (2012) Synthesis of WO_3@Graphene composite for enhanced photocatalytic oxygen evolution from water. RSC Adv 2:1356–1363
29. Ng YH, Iwase A, Bell NJ, Kudo A, Amal R (2011) Semiconductor/reduced graphene oxide nanocomposites derived from photocatalytic reactions. Catal Today 164:353–357
30. Li B, Zhang Y, Zou R, Wang Q, Zhang B, An L, Yin F, Hua Y, Hu J (2014) Self-assembled WO_{3-x} hierarchical nanostructures for photothermal therapy with a 915 nm laser rather than the common 980 nm laser. Dalton Trans 43:6244–6250
31. Bu Y, Chen Z, Yu J, Li W (2013) A novel application of g-C_3N_4 thin film in photoelectrochemical anticorrosion. Electrochim Acta 88:294–300
32. Gu Z, Zhai T, Gao B, Sheng X, Wang Y, Fu H, Ma Y, Yao J (2006) Controllable assembly of WO_3 nanorods/nanowires into hierarchical nanostructures. J Phys Chem B 110:23829–23836
33. Wang P, Bai Y, Luo P, Liu J (2013) Graphene-WO_3 nanobelt composite: elevated conduction band toward photocatalytic reduction of CO_2 into hydrocarbon fuels. Catal Commun 38:82–85
34. Thangavel S, Elayaperumal M, Venugopal G (2012) Synthesis and properties of tungsten oxide and reduced graphene oxide nanocomposites. Mater Express 2:327–334
35. Zhi M, Huang W, Shi Q, Wang M, Wang Q (2016) Sol–gel fabrication WO_3/RGO nanocomposite film with enhanced electrochromic performance. RSC Adv 6:67488–67494
36. Lin J, Hu P, Zhang Y, Fan M, He Z, Ngaw C, Loo J, Liao D, Tan T (2013) Understanding the photoelectrochemical properties of a reduced graphene oxide-WO_3 heterojunction photoanode for efficient solar-light-driven overall water splitting. RSC Adv 3:9330–9336
37. Zhang L, Liang J, Huang Y, Ma Y, Wang Y, Chen Y (2009) Size-controlled synthesis of graphene oxide sheets on a large scale using chemical exfoliation. Carbon 47:3365–3368
38. Wang F, Wang Y, Zhan X, Safdar M, Gong J, He J (2014) Pt nanoparticle and CdS quantum dot assisted WO_3 nanowires grown on flexible carbon fibers for efficient oxygen production. CrystEngComm 16:1389–1394
39. Dupin J, Gonbeau D, Vinatier P, Levasseur A (2000) Systematic XPS studies of metal oxides, hydroxides and peroxides. Phys Chem Chem Phys 2:1319–1324
40. Song J, Huang Z, Pan L, Zou J, Zhang X, Wang L (2015) Oxygen-deficient tungsten oxide as versatile and efficient hydrogenation catalyst. ACS Catal 5:6594–6599
41. Zhu W, Sun F, Goei R, Zhou Y (2017) Facile fabrication of RGO-WO_3 composites for effective visible light photocatalytic degradation of sulfamethoxazole. Appl Catal B-Environ 207:93–102
42. Stankovich S, Dikin DA, Piner RD, Kohlhaas KA, Kleinhammes A, Jia Y, Wu Y, Nguyen SBT, Ruoff RS (2007) Synthesis of graphene-based nanosheets via chemical reduction of exfoliated graphite oxide. Carbon 45:1558–1565
43. Yang D, Velamakanni A, Bozoklu G, Park S, Stoller M, Piner RD, Stankovich S, Jung I, Field DA, Ventrice CA (2009) Chemical analysis of graphene oxide films after heat and chemical treatments by X-ray photoelectron and Micro-Raman spectroscopy. Carbon 47:145–152
44. Wang S, Chen T, Rao KK, Wong M (2007) Nanocolumnar titania thin films uniquely incorporated with carbon for visible light photocatalysis. Appl Catal B-Environ 76:328–334
45. Tuinstra FF, Lo Koenig J (1970) Raman spectra of graphite. J Chem Phys 53:1126–1130

46. Srivastava S, Jain K, Singh V, Singh S, Vijayan N, Dilawar N, Gupta G, Senguttuvan T (2012) Faster response of NO_2 sensing in graphene-WO_3 nanocomposites. Nanotechnology 23:205501 (1–7)
47. Casiraghi C, Pisana S, Novoselov K, Geim A, Ferrari A (2007) Raman fingerprint of charged impurities in graphene. Appl Phys Lett 91:233108
48. Graf D, Molitor F, Ensslin K, Stampfer C, Jungen A, Hierold C, Wirtz L (2007) Spatially resolved Raman spectroscopy of single- and few-layer graphene. Nano Lett 7:238–242